ADVANCED MATERIALS
www.advmat.de

Highly Efficient Light-Emitting Diodes Based on Self-Assembled Colloidal Quantum Wells

Yunke Zhu, Yunzhou Deng, Peng Bai, Xinan Wu, Yige Yao, Qinyun Liu, Jingjing Qiu, An Hu, Zhenyu Tang, Wenjin Yu, Yaolong Li, Pengzuo Jiang, Zhetong Liu, Peng Gao, Yanlei Hao, Wangxiao Jin, Desui Chen, Xitong Zhu, Yizheng Jin, and Yunan Gao**

Nanocrystal-based light-emitting diodes (Nc-LEDs) have immense potential for next-generation high-definition displays and lighting applications. They offer numerous advantages, such as low cost, high luminous efficiency, narrow emission, and long lifetime. However, the external quantum efficiency (EQE) of Nc-LEDs, typically employing isotropic nanocrystals, is limited by the out-coupling factor. Here efficient, bright, and long lifetime red Nc-LEDs based on anisotropic nanocrystals of colloidal quantum wells (CQWs) are demonstrated. Through modification of the substrate's surface properties and control of the interactions among CQWs, a self-assembled layer with an exceptionally high distribution of in-plane transitions dipole moment of 95%, resulting in an out-coupling factor of 37% is successfully spin-coated. The devices exhibit a remarkable peak EQE of 26.9%, accompanied by a maximum brightness of 55 754 cd m^{-2} and a long operational lifetime (T_{95}@100 cd m^{-2}) over 15 000 h. These achievements represent a significant advancement compared to previous studies on Nc-LEDs incorporating anisotropic nanocrystals. The work is expected to provide a general self-assembly strategy for enhancing the light extraction efficiency of Nc-LEDs based on anisotropic nanocrystals.

1. Introduction

Solution-processable colloidal nanocrystals with emission-wavelength tunability, narrow emission linewidth, nearly unity photoluminescence quantum yield (PLQY), and electrical stability have become a superb semiconductor material for light-emitting diode (LED) and laser applications.[1–12] Significant progress has been made in Nc-LEDs over the past decades, achieving a high external quantum efficiency (EQE) close to ≈30%[3,11,13] and long operational lifetimes exceeding 100 000 h (T_{95}@100 cd m^{-2}, the time when the luminance decays to 95% of the initial value of 100 cd m^{-2}).[3,14] The PLQY of nanocrystals as the light-emitting layer in Nc-LEDs has approached 100%, and charge carrier injection has been optimized. However, further enhancement of EQE in Nc-LEDs is impeded by the out-coupling factor, a critical parameter determining the maximum light extraction efficiency from the device.[15,16] Typically, the horizontal transitions dipole moment (TDM) of isotropic nanocrystals predominantly contributes to light emitting, while the vertical TDM contribute negligibly due to their strong coupling with the surface-plasmon mode of the metal electrodes.[16] Therefore, enhancing the ratio of horizontally oriented TDM has long been regarded as a method to improve the light out-coupling and raise the upper limit of the EQE in

Y. Zhu, P. Bai, X. Wu, Y. Yao, Q. Liu, J. Qiu, A. Hu, Z. Tang, W. Yu, Y. Li, P. Jiang, Y. Gao
State Key Laboratory for Mesoscopic Physics and Frontiers Science Center for Nano-Optoelectronics
School of Physics
Peking University
Beijing 100871, China
E-mail: gyn@pku.edu.cn

Y. Deng
State Key Laboratory of Modern Optical Instrumentation
College of Optical Science and Engineering
International Research Center for Advanced Photonics
Zhejiang University
Hangzhou 310027, China

Y. Deng
Cavendish Laboratory
University of Cambridge
Cambridge CB3 0HE, UK

Z. Liu, P. Gao
Electron Microscopy Laboratory
School of Physics
Peking University
Beijing 100871, China

Y. Hao, W. Jin, D. Chen, X. Zhu, Y. Jin
Key Laboratory of Excited-State Materials of Zhejiang Province
State Key Laboratory of Silicon and Advanced Semiconductor Materials
Department of Chemistry
Zhejiang University
Hangzhou 310027, China
E-mail: yizhengjin@zju.edu.cn

The ORCID identification number(s) for the author(s) of this article can be found under https://doi.org/10.1002/adma.202305382

DOI: 10.1002/adma.202305382

Nc-LEDs.[17,18] Although self-assembly has been demonstrated to manipulate the TDM orientation of anisotropic nanocrystals, especially colloidal quantum wells (CQWs),[19–21] it remains challenging to successfully incorporate them into Nc-LEDs for enhanced performance.

The strong quantum confinement[22] in the vertical direction endows the CQWs with the unique optical property of pure in-plane TDM distribution.[16,23–25] However, this advantage has not been successively exploited. Some efforts have been made to develop CQW-LEDs,[21,26–33] and red CQW-LEDs perform much better than green and blue ones, due to the core/shell structure of red CQWs with excellent optoelectronic properties. In 2014, Chen et al. reported the first red LED based on core/shell CQWs.[33] In 2020, Liu et al. improved EQE to 19.2% by constructing an inverted-structure device with better carrier balancing, accompanied with a maximum luminance of 23 490 cd m^{-2}.[26] Baruj et al. recently reported the devices with peak EQE of 18.1% by liquid–air interface self-assembly approach.[34] However, the overall performance of CQW-LEDs (EQE < 20%; T_{95}@100 cd m^{-2} < 100 h, Table S2, Supporting Information) still falls short of their upper limits endowed by the asymmetric shape and pure in-plane TDM. In organic light-emitting diodes, aligning the dipole orientation to be horizontal has proven effective in achieving EQE of nearly 40%.[35–40]

Here, we report the high efficiency, bright, and long lifetime CQW-LEDs achieved through successful manipulation of the TDM orientation. We reveal that optimizing the flatness of the substrate and adjusting the concentration of solution to reduce the interaction between CQWs facilitate the formation of a self-assembled monolayer during spin-coating. We fabricated the normal-structure devices with a monolayer emitting layer (EML) by using direct spin-coating and in situ self-assembly of CQWs all oriented "face-down." Compared to the isotropic emitters with an in-plane TDM ratio of only 67%, the CQWs EML exhibits a significantly higher in-plane TDM ratio of ≈95%. Moreover, we incorporated a novel hole transfer layer (HTL) material reported recently,[3] which effectively suppressed electron leakage during device operation. These combined strategies finally led to the best performance among CQW-LEDs with a peak EQE of 26.9%, along with an enhanced out-coupling factor of 37%.

2. Results and Discussion

In recent years, the synthesis of red (CdSe/CdZnS) core/shell CQWs was continuously optimized showing good stability and unity PLQY.[41,42] By referring to previous works,[26] we synthesized CQWs with uniform particle size and regular rectangular shape (Figure S1, Supporting Information). These inherent morphological features render CQWs quite advantageous in self-assembly to "face-down" orientation on the substrate, as directly observed in the transmission electron microscope (TEM) images (**Figure 1**a). Previous studies have shown that II-VI CQWs exhibit a pure in-plane distribution of TDM due to the strong one-dimensionally quantum confinement in the normal direction of the CQWs[23,24] indicating that we can control the TDM orientation of the EML by manipulating the self-assembly of anisotropic nanocrystals. Assuming a conventionally normal-structure device with CQWs as the EML oriented "face-down" or "edge-up" (Figure 1b), the former configuration ensures that the dipole moments are exclusively distributed in-plane, setting it apart from isotropic nanocrystals.[16] The spatial arrangement of the CQWs influences the directionality of the exciton radiation. We calculate the effect of TDM orientation on the EQE of CQW-LEDs using the finite difference time domain method. When the dipole moments are horizontally oriented, ≈37% of the emitted energy is directed into the air (Figure 1c) with an optimized distance between the emitter and electrode. The remaining energy is distributed among various emission channels, including waveguide mode (≈14%), emission to the substrate (≈32%), surface-plasmon mode (≈15%), and absorption (≈2%). Conversely, by orienting the CQWs in a random manner (Figure 1d), the energy emitted into the air decreases to only ≈26% (with 30% attributed to the surface-plasmon mode) due to the negligible contribution from vertical TDMs (Figure S3, Supporting Information). Therefore, manipulating the TDM distribution to be horizontal is the key to boosting the light extraction efficiency.

Self-assembly of CQWs has been conducted with several methods including inkjet printing[19] and liquid–air interface self-assembly.[20,24,43,44] However, these approaches are difficult to be incorporated with Nc-LEDs devices. The spin-coating method is widely utilized for the development of high-performance Nc-LEDs, and our previous studies show that this technique can also realize the self-assembly of CQWs with high horizontal TDM distribution.[21] The self-assembly process is significantly affected by the surface properties of the substrate as well as the interaction among CQWs.[19,21] In order to incorporate them into devices, we investigated the self-assembly of CQWs on commonly used carrier transfer layers.

We first found that the flatness of the substrate-transport layer interface can significantly impact the controllable arrangement of the CQWs. Most previous works on CQW-LEDs utilized an inverted-structure device with ZnO-like nanocrystals as an electron transfer layer (ETL) beneath the EML.[26,28,45,46] For spin-coated $Zn_{0.9}Mg_{0.1}O$ films of ≈50 nm thickness on a quartz substrate, we determined the root-mean-square (RMS) of height ≈1.304 nm (Figure S4, Supporting Information) using atomic force microscopy (AFM). The $Zn_{0.9}Mg_{0.1}O$ nanoparticles resulted in substantial surface unevenness, which may impede the ordered alignment of CQWs during deposition (**Figure 2**a). On the contrary, the HTL represented by the polymeric organic polymer, such as poly((9,9-dioctylfluorenyl-2,7-diyl)-co-(4,4′-(*N*-(4-*sec*-butylphenyl)diphenylamine))) (TFB) and poly((9,9-dioctylfluorenyl-2,7-diyl)-*alt*-(9-(2-ethylhexyl)-carbazole-3,6-diyl)) (PF8Cz), can efficiently form films with a much higher flatness (Figure S4, Supporting Information, RMS ≈0.253 nm). As a result, we found that when the CQWs layer was spin-coated on top of the polymeric HTL, it displayed exceptional film formation (RMS < 1 nm) compared to using $Zn_{0.9}Mg_{0.1}O$ as substrate (RMS > 2 nm) (Figure 2b). The excellent CQWs film's flatness

Y. Gao
Peking University Yangtze Delta Instituteof Optoelectronics
Peking University
Nantong 226010, China
Y. Gao
Collaborative Innovation Center of Extreme Optics
Shanxi University
Taiyuan 030006, China

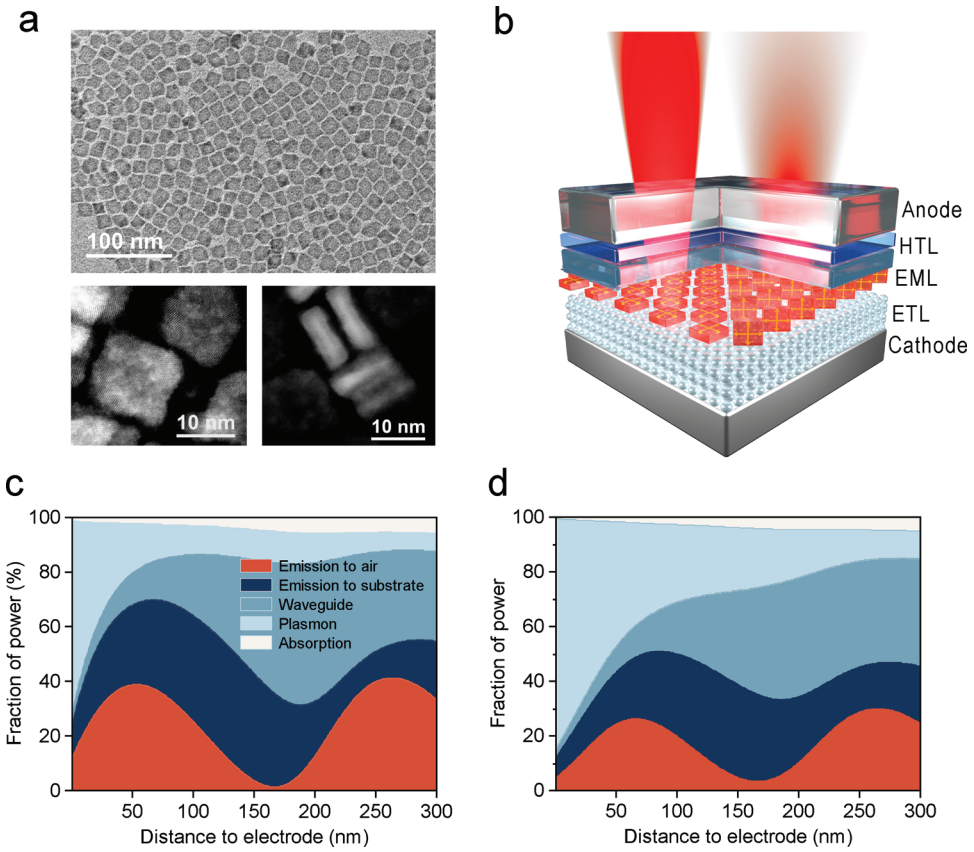

Figure 1. a) TEM image of CdSe/CdZnS core/shell CQWs. The high-angle annular dark-field (HADDF) images below show the nanocrystal oriented "face-down" and "edge-up." b) Schematic illustration of the device with the normal-structure of Anode/HTL/EML/ETL/Cathode. CQWs are used as EML oriented "face-down" or "edge-up." Optical mode analysis of CQW-LEDs depending on horizontal dipole orientation c) and random dipole orientation d).

below the nanometer scale may facilitate the self-assembly of the EML.

The interaction between CQWs themselves plays another crucial role in their self-assembly. In the saturated aliphatic hydrocarbon solvent, the synthesized CQWs with oleic carboxylate ligands (Figure S1, Supporting Information) show good dispersion and stability. Previous studies have shown that CQWs tend to orient "face-down" during solvent evaporation to minimize potential energy while they also exhibit stacking tendencies in highly concentrated solutions due to molecular forces between nanocrystal-ligand complexes.[21,44] Therefore, adjusting the concentration of CQWs and the design of the ligands provide a simple and effective approach to manipulate their self-assembly on ETL and HTL surfaces.

To examine the TDM distribution of the CQW films, we used back focal plane (BFP) imaging (Figure S5, Supporting Information). This technique has been commonly employed to determine TDMs in various materials, including single molecule, van der Waals materials, and CQW.[23,24,47–49] The presence of pure in-plane and vertical TDMs result leads to characteristic images resulting from interlayer reflections and interferences, which can be accurately quantified through numerical modeling[19,23,24] (Figure S6, Supporting Information). By comparing the experimental results with theoretical simulations (Figure S7, Supporting Information), we found that the CQWs films spin-coated on PF8Cz substrate with higher flatness and a lower concentration of 8 mg mL^{-1} exhibited the highest in-plane TDM distribution of 95% (Figure 2d; top). In contrast, films with the same low concentration on $Zn_{0.9}Mg_{0.1}O$ substrates achieved a maximum distribution of only 85%. This disparity proves that surface flatness indeed significantly impacts CQWs self-assembly, as illustrated in Figure 2a. Moreover, in thicker CQWs films prepared with increasing concentration, the in-plane TDM distribution gradually decreases to 70%, approaching the characteristics of an isotropic emitter with an in-plane TDM ratio of 67%. This indicates that the CWQs progressively stacked, without a preferred orientation. The presence of a 95% in-plane TDM distribution in the CQW film suggests that a vast majority of them self-assemble in a "face-down" orientation on the PF8Cz HTL. We also demonstrated the generality of the approach for realizing CQWs self-assembly on different organic HTLs, with films exhibiting high in-plane TDM distribution (>90%) on poly(9-vinylcarbazole) (PVK), poly(*N*,*N*′-bis(4-butylphenyl)*N*,*N*′-bis(phenyl)-benzidine) (Poly-TPD), and TFB (Figure S8, Supporting Information). We obtained different nanocrystal-ligand complexes by ligand exchange and demonstrated the importance of ligands for self-assembly of CQWs. The findings demonstrate that nanocrystals equipped with ligands of varying chain lengths

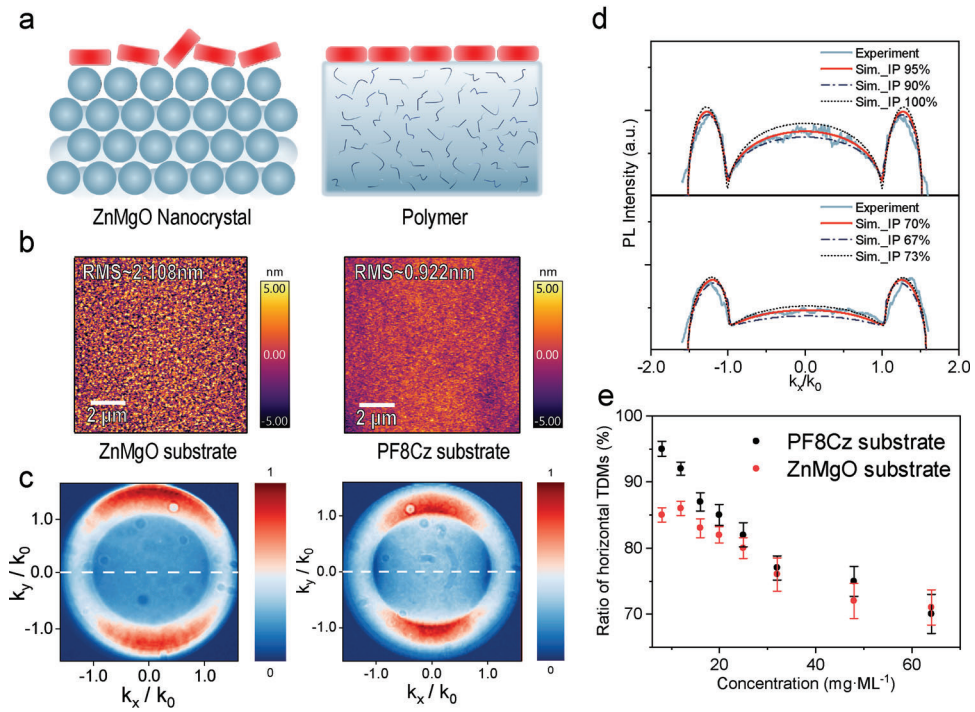

Figure 2. a) Schematic illustration of the arrangement of CQWs on different substrates. AFM images of CQWs films on the substrate as $Zn_{0.9}Mg_{0.1}O$ (b; left) and PF8Cz (b; right). Experimental back focus plane images with a solution concentration of 8 mg mL^{-1} (c; left) and 64 mg mL^{-1} (c; right). d) Comparison between experiment and simulated line cuts along the dashed white lines. e) TDMs distribution of films prepared by spin coating on substrates of PF8Cz and $Zn_{0.9}Mg_{0.1}O$ with different solutions concentration.

exhibit the capacity to self-assemble within solutions of low concentration (Figure S9, Supporting Information).

We fabricated CQW-LEDs with a normal structure based on CQW as EML with high in-plane TDM distribution. The devices (**Figure 3**a) consisted of multiple layers of, in the following order, indium tin oxide (ITO)-coated glass substrates, poly(ethylenedioxythiophene):polystyrene sulphonate (PEDOT:PSS, ≈30 nm), PF8Cz (≈40 nm), CdSe/CdZnS core/shell CQWs (≈5 nm), $Zn_{0.9}Mg_{0.1}O$ (≈80 nm), and silver electrodes (≈100 nm). A cross-sectional high-angle annular dark-field scanning transmission electron microscopy (HAADF-STEM) image (Figure 3b) reveals the device structure and directly confirms the self-assembly of CQWs when only a monolayer is spin-coated at a concentration of 8 mg mL^{-1}. This observation validates the earlier determination of high in-plane distribution using the optical method of BFP imaging. Individual CQWs are arranged in a "face down" orientation, with each CQW positioned adjacent to the next one and separated by ligands, as shown in zoomed-in the STEM figure (Figure 3c).

Devices based on monolayer CQWs as the EML (Figure 3c; and Figure S11, Supporting Information) might be susceptible to electron leakage from the EML to charge-transport layers. One strategy to boost EQE in such a device is to utilize HTLs with better electron-blocking properties. Recently, Deng et al. reported a tailored polymer HTL, PF8Cz, that effectively eliminates electron leakage across the interface between the EML and HTL.[3] The PF8Cz polymer contains rigid and planar carbazole unit that is copolymerized with fluorene unit. This feature which leads to shallower lowest-unoccupied molecular orbital energy level effectively suppressed disorder compared to TFB[3] (Figure 3d; and Figure S12, Supporting Information) which shall enable a larger energy barrier for electron transfer from the CQWs to PF8Cz (arrows, Figure 3d). We use the same device structure to compare the device performance based on TFB or PF8Cz. The TFB-based device exhibited parasitic emission in the EL spectra (Figure 3e; and Figure S13 (Supporting Information) shows the PL properties of TFB), suggesting the injection of electrons into the HTL. In contrast, the PF8Cz-based device shows pure emission, indicating successful suppression of electron leakage. With the aforementioned optimization, the red PF8Cz-based devices achieved peak EQEs of 26.9% at a voltage of 2.30 V (Figure 3f), setting a new efficiency record among CQW-LEDs (Table S2, Supporting Information). This performance significantly surpassed that of TFB-based devices. We also fabricated CQW-LEDs with lower in-plane TDM distribution, which exhibit lower efficiency (Figure S16, Supporting Information). The result indicated the facilitated out-coupling factor by self-assembly. We calculated the variation of the device's EQE with the PLQY of CQWs and the ratio of horizontal TDM and plotted contour maps (Figure 3h). The PLQY of CQWs, with the encapsulation of a wide bandgap shell layer and inorganic–organic interfacial passivation, remained ≈100% in solution, ≈82% in a thin film on quartz, and ≈71% on $Zn_{0.9}Mg_{0.1}O$ nanocrystal film (Figure 3g). Considering that the PLQY of our CQWs film on $Zn_{0.9}Mg_{0.1}O$ nanocrystal film is ≈71%, our optical simulation predicts a peak EQEs of 27.2%, which agrees well with the experiment results. The result suggests an exceptionally high out-coupling factor of 0.37.

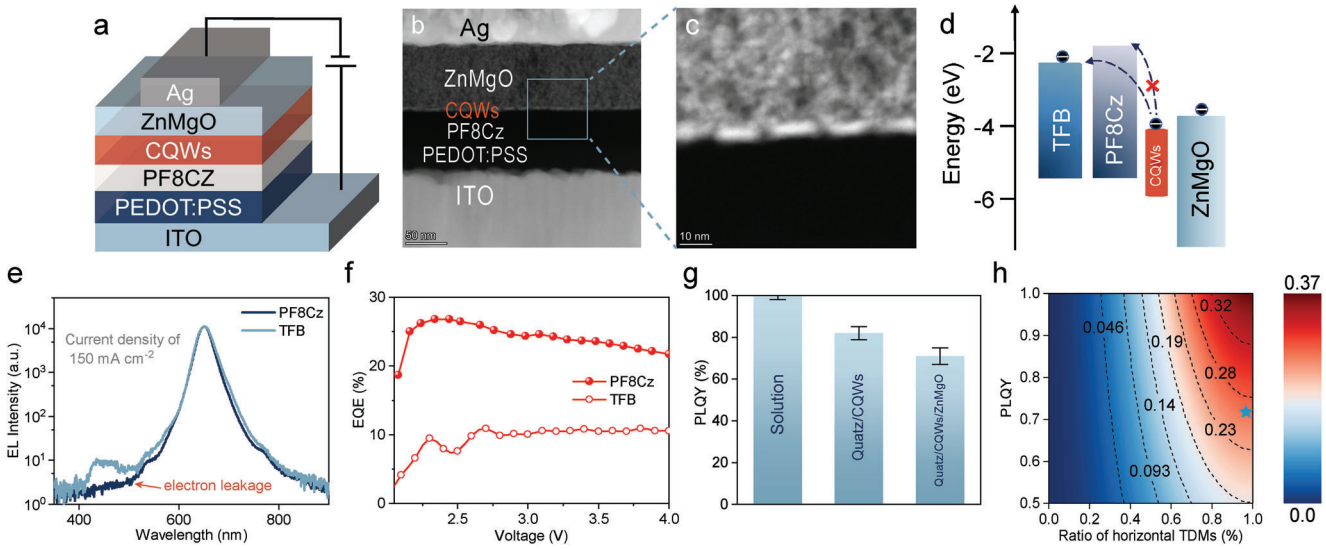

Figure 3. a) Device structure of CQW-LED. b) The cross-sectional high-angle annular dark-field scanning transmission electron microscopy (HAADF-STEM) image of CQW-LED. c) Zoom-in image of b). d) Schematic diagram of electronic transport in devices based on TFB or PF8Cz. The PF8Cz-based device effectively blocked electron leakage from EML to HTL. e) EL spectra of the CQW-LED (semilog scale) measured at a current density of 150 mA cm^{-2}. The parasitic emissions from TFB HTL are indicated by the arrows. f) EQE-voltage relationship of the PF8Cz-based and TFB-based device with a peak EQE of 26.9% and 10.8%. g) The PLQY of CQWs films on different substrates. Tests were conducted under an air atmosphere. h) Contour plot of the simulation results of device EQEs as a function of PLQY and the ratio of horizontal TDMs of CQWs emissive layer. The asterisk represents the maximum EQE of the simulation.

The fabricated PF8Cz-based device exhibits a sub-bandgap turn-on voltage of 1.80 V (**Figure 4**a), similar to previously reported red Nc-LEDs with efficient charge injection.[3,6,11] With excellent charge balance performance and light extraction efficiency, the devices in this batch achieve a maximum luminescence of 55 754 cd m^{-2} (Figure S17, Supporting Information), surpassing previously reported CQW-LEDs (Table S1, Supporting Information). As shown in Figure 4b, the electroluminescence spectrum of the device hardly changed until the voltage rises to 8 V, with Commission Internationale de l'Eclairage (CIE) coordinates showing minimal variation with increasing luminance (Figure S18, Supporting Information). At a display-related luminance of 1000 cd m^{-2}, the CIE coordinates are (0.708, 0.289) (Figure 4c), indicating that the color gamut covers 100% of the International Telecommunication Union Recommendation BT 2020 (Rec. 2020) standard. The angular emission intensity of our CQW-LEDs follows a Lambertian profile (Figure 4d). The histogram of 25 devices indicates an average peak EQE of 23.6% with a low relative standard deviation of 1.4% (Figure 4e). Elimination of parasitic emission with negative effects and excellent carrier balance enhanced the stability of devices. The lifetime is evaluated by measuring luminance over time at an initial luminance of 1000 cd m^{-2}. The results are fitted by an empirical equation, $(L_0)^n \times T_{95} = \text{constant}$, where L_0, n, and T_{95} are initial brightness, acceleration factor, and lifetime (the time required for the luminance to decrease to 0.95 L_0), respectively. The acceleration factor, n, is determined to be ≈1.9 according to the reference.[3] Based on the measured T_{95}@1000 cd m^{-2} of ≈200 h (Figure 4f), the fitting estimates that T_{95}@100 cd m^{-2} is over 15 000 h, demonstrating the devices' excellent stability and their potential to reach commercially available levels[14,50] (T_{95}@100 cd m^{-2} ≈100 000 h). The stability of the device can also be demonstrated by the fact that the performance of the device does not change significantly under repetitive measurements (Figure S19, Supporting Information). According to a comparison of several key metrics (Table S2, Supporting Information), the overall performance of our red devices surpasses that of previously reported solution-processed CQW-LEDs.

3. Conclusion

The present work represents a significant breakthrough in the field of CQW-LEDs by achieving record-high efficiency and excellent operational stability through the self-assembly of anisotropic nanocrystals. This is the first report demonstrating that the EQEs of CQW-LEDs can exceed 20% by modulating the in-plane TDM distribution. The near unity in-plane TDM distribution achieved in our devices enables a light extraction ratio close to the limit of ≈0.37. However, there is still a theoretical potential for further improving the maximum efficiency by enhancing the PLQY of the film, and the operational lifetime needs further development to meet application requirements, requiring more efforts on CQW synthesis. The success of this work with anisotropic nanocrystals can be readily extended to other color regions, opening up possibilities for various applications of anisotropic nanocrystal materials. This work provides a pioneering guide for the utilization of anisotropic nanocrystals in diverse fields of nanocrystal synthesis, self-assembly, nanocrystal-based display, and lighting.

4. Experimental Section

Chemicals: Chemicals were used directly without any purification: selenium powder (Se, 200mesh, Sigma-Aldrich 99.999%), 1-octadecene

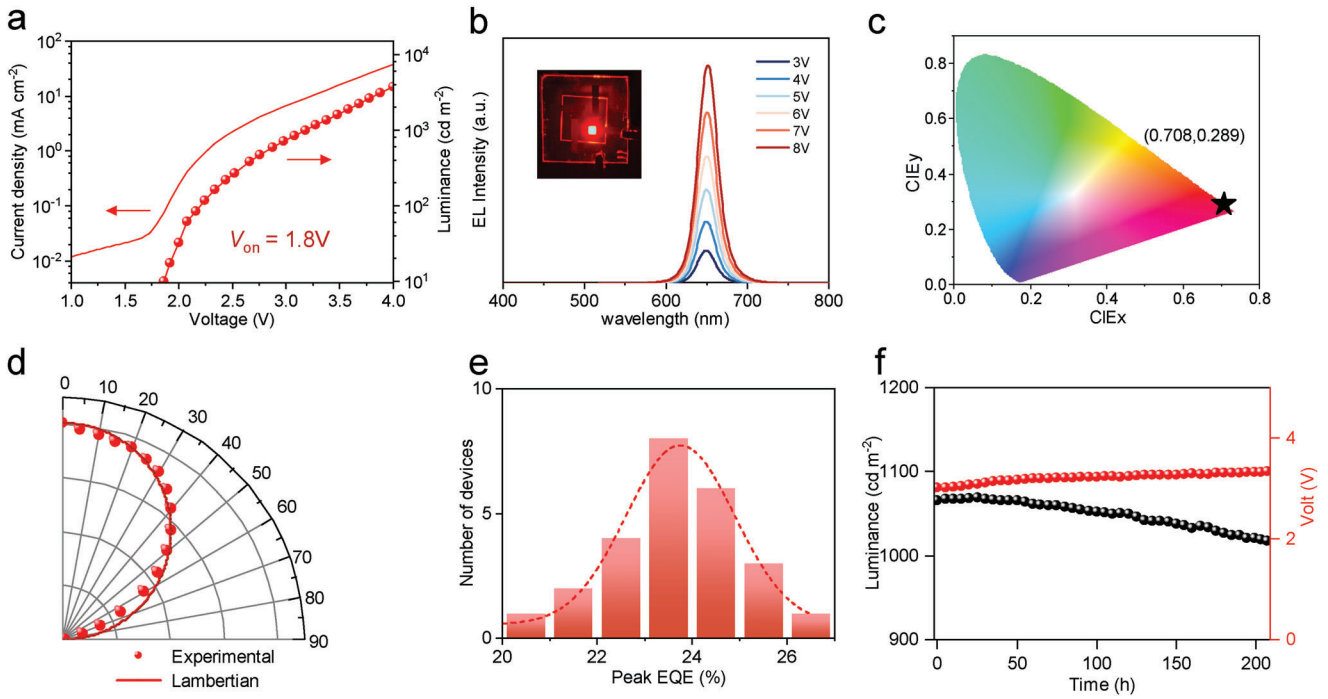

Figure 4. a) Current density-luminance-voltage characteristics of a PF8Cz-based device. b) EL spectra of CQW-LEDs under different biases. Inset shows the operating CQW-LED. c) The CIE 1931 coordinates of CdSe/CdZnS core/shell CQW-LEDs. d) Angular distribution of the EL intensity follows the Lambertian profile. e) Histogram of peak EQEs from 25 devices. f) Luminance and voltage as a function of operation time for a device. Device lifetime is evaluated by measuring luminance over time at constant current density.

(ODE, Sigma-Aldrich 90%), oleic acid (OAc, Sigma-Aldrich 90%), oleylamine (OLA, Sigma-Aldrich 70%), dimethyl sulfoxide (DMSO, Alfa Aesar), cadmium acetate dihydrate (Sigma-Aldrich 98%), cadmium acetate ($Cd(Ac)_2$, Macklin 99.995%), zinc acetate ($Zn(Ac)_2$, Alfa Aesar 99.9%), magnesium acetate ($Mg(Ac)_2$, Acros 99.997%), Tetramethylammonium hydroxide pentahydrate (Acros 98%), 1-octanethiol (Sigma-Aldrich ≥98.5%), sodium myristate (TCI 98%), cadmium nitrate tetrahydrate (Sigma-Aldrich 99%), hexane (Honeywell HPLC), octane (Sigma-Aldrich ≥98.5%), methanol (Fisher HPLC), ethanol (EtOH, Fisher HPLC), TFB, and PF8Cz (Volt-Amp Optoelectronics Tech. Co., Ltd, Dongguan, China).

Precursor Preparation: Cadmium myristate ($Cd(myristate)_2$) was synthesized as follows, cadmium nitrate tetrahydrate (1.23 g) was dissolved in methanol (40 mL), and sodium myristate (3.13 g) was dissolved in methanol (250 mL). Two chemicals were fully dissolved with the help of sonication for 20 min, and the two solutions were mixed. After 2 min, the resulting white precipitate of $Cd(myristate)_2$ was filtered and rinsed 5 times with fresh methanol. Finally, the $Cd(myristate)_2$ was dried under a vacuum overnight.

4 ML CdSe Core CQWs Synthesis: 4 ML CdSe core CQWs were synthesized according to the protocol presented in the literature with slight modifications.[42] 340 mg of Cadmium myristate and 24 mg of Se in ODE (30 mL) were degassed at 100 °C for 10 min in a 50 mL three-neck flask. Then the mixture was heated up with the target temperature of 240 °C. When the temperature reached 195 °C, 80 mg cadmium acetate dihydrate was swiftly added to the flask. After 10 min growth at 240 °C, the reaction was cooled down to room temperature with the addition of 1 mL of OAc. The resulting CdSe core CQWs were cleaned twice with hexane and ethanol.

CdSe/CdZnS Core/Shell CQWs Synthesis: CdSe/CdZnS core/shell CQWs were synthesized according to the protocol presented in the literature with slight modifications.[42] A certain amount of 4 ML CdSe core CQWs, 23.06 mg $Cd(Ac)_2$, 55.04 mg $Zn(Ac)_2$, and 7.5 mL of ODE. 1 mL of OAc were added to a 50 mL three-neck flask. Then the mixture was degassed under a vacuum for 60 min at 85 °C. Afterward, 1 mL of OLA was added, and the temperature was raised to 305 °C under N_2 at a rate of ≈18 °C min^{-1}. Starting at 162 °C, a solution of 140 µL 1-octaethiol dissolved in 5 mL of ODE was injected at a rate of 5 mL h^{-1}. After the temperature reached 305 °C, it was kept at this temperature for 40 min and then the reaction was cooled down by a nitrogen gun. 5 mL of hexane was added at 50 °C. Synthesized core/shell CQWs were cleaned once with ethanol, acetone, and methanol for each and dispersed in octane.

Synthesis of $Zn_{0.9}Mg_{0.1}O$ Nanocrystals: Colloidal $Zn_{0.9}Mg_{0.1}O$ nanocrystals were synthesized by the dropwise addition of an ethanol solution (10 mL) of tetramethylammonium hydroxide (5 mmol) into a dimethyl sulfoxide solution of zinc acetate hydrate (2.7 mmol) and magnesium acetate hydrate (0.3 mmol) at 50 °C. The solution was stirred for 1 h at 50 °C in ambient conditions. The $Zn_{0.9}Mg_{0.1}O$ nanocrystals were precipitated from the solution by adding ethyl acetate and then dispersed in ethanol.

Device Fabrication: ITO-coated glass slides with a resistance of ≈20 Ω sq^{-1} were processed by ultrasonic cleaning and oxygen plasma before the deposition of materials. PEDOT:PSS solutions (Baytron PVP Al 4083) were spin-coated onto the ITO-coated glass at 4000 rpm for 45 s and baked at 150 °C for 30 min. The substrates were transferred into a nitrogen-filled glove box ($O_2 \leq 1$ ppm, $H_2O \leq 1$ ppm). TFB or PF8Cz solutions in chlorobenzene (12 mg mL^{-1}) were spin-coated at 2000 rpm for 45 s and baked at 150 °C for 30 min to form the HTLs. CQW solutions in octane $^{-1}$were spin-coated at 2000 rpm for 45 s. $Zn_{0.9}Mg_{0.1}O$ nanocrystals in ethanol (≈30 mg mL^{-1}) were spin-coated onto the CQW layers at 2000 rpm for 45 s and baked at 85 °C for 30 min. Finally, Ag electrodes (100 nm) were deposited by thermal evaporation in a high vacuum (≈10^{-7} torr). The devices were encapsulated in a glove box by using an ultraviolet-curable resin. The active size of the CQW-LEDs is 4 mm^2.

Characterization: The time-resolved photoluminescence was measured by a time-correlated single-photon counting (TCSPC)

spectrofluorometer (FLS1000, Edinburgh Instrument). The absolute PLQY of samples was measured on a spectrum calibrated system (FLS1000, Edinburgh) including a Xe lamp, integrating sphere, and visible photomultiplier tube. XRD was measured by Rigaku SmartLab SE. FTIR was measured by IRAFFINITY-1. TEM was measured by FEI Tecnai T20. AFM was measured by Asylum Research Cypher ES. The HAADF-STEM and EDS-STEM measurements were conducted on an aberration-corrected FEI Titan Themis G2 microscope with an accelerating voltage of 300 kV. BFP was measured by an oil-immersion objective (CFI Apo TIRF 60XC Oil) under the excitation of a 405 nm diode laser.

Supporting Information

Supporting Information is available from the Wiley Online Library or from the author.

Acknowledgements

Y.Z. and Y.D. contributed equally to this work. This work was supported by the National Key Research and Development Program of China (Grant No. 2018YFA0306302, Grant No.2021YFB3602703, Grant No.2022YFB3606503), the National Natural Science Foundation of China (Grant No. 62375004, 61875002, Grant No.21975220), the Beijing Natural Science Foundation (Grant No. Z190005), the Fundamental Research Funds for the Central Universities, and the Key Research and Development Program of Zhejiang Province (2021C01030). We acknowledge the Electron Microscopy Laboratory of Peking University for the use of electron microscopes.

Conflict of Interest

The authors declare no conflict of interest.

Data Availability Statement

The data that support the findings of this study are available from the corresponding author upon reasonable request.

Keywords

anisotropic nanocrystal, colloidal quantum wells, external quantum efficiency, light-emitting diodes, transition dipole moments

Received: June 5, 2023
Revised: August 31, 2023
Published online:

[1] Y.-H. Won, O. Cho, T. Kim, D.-Y. Chung, T. Kim, H. Chung, H. Jang, J. Lee, D. Kim, E. Jang, *Nature* **2019**, *575*, 634.
[2] T. Kim, K.-H. Kim, S. Kim, S.-M. Choi, H. Jang, H.-K. Seo, H. Lee, D.-Y. Chung, E. Jang, *Nature* **2020**, *586*, 385.
[3] Y. Deng, F. Peng, Y. Lu, X. Zhu, W. Jin, J. Qiu, J. Dong, Y. Hao, D. Di, Y. Gao, T. Sun, M. Zhang, F. Liu, L. Wang, L. Ying, F. Huang, Y. Jin, *Nat. Photonics* **2022**, *16*, 505.
[4] B. S. Mashford, M. Stevenson, Z. Popovic, C. Hamilton, Z. Zhou, C. Breen, J. Steckel, V. Bulovic, M. Bawendi, S. Coe-Sullivan, P. T. Kazlas, *Nat. Photonics* **2013**, *7*, 407.
[5] X. Dai, Z. Zhang, Y. Jin, Y. Niu, H. Cao, X. Liang, L. Chen, J. Wang, X. Peng, *Nature* **2014**, *515*, 96.
[6] Z. Zhang, Y. Ye, C. Pu, Y. Deng, X. Dai, X. Chen, D. Chen, X. Zheng, Y. Gao, W. Fang, X. Peng, Y. Jin, *Adv. Mater.* **2018**, *30*, 1801387.
[7] D. Chen, D. Chen, X. Dai, Z. Zhang, J. Lin, Y. Deng, Y. Hao, C. Zhang, H. Zhu, F. Gao, Y. Jin, *Adv. Mater.* **2020**, *32*, 2006178.
[8] J. Lin, X. Dai, X. Liang, D. Chen, X. Zheng, Y. Li, Y. Deng, H. Du, Y. Ye, D. Chen, C. Lin, L. Ma, Q. Bao, H. Zhang, L. Wang, X. Peng, Y. Jin, *Adv. Funct. Mater.* **2020**, *30*, 1907265.
[9] C. Pu, X. Dai, Y. Shu, M. Zhu, Y. Deng, Y. Jin, X. Peng, *Nat. Commun.* **2020**, *11*, 937.
[10] Y. Altintas, U. Quliyeva, K. Gungor, O. Erdem, Y. Kelestemur, E. Mutlugun, M. V. Kovalenko, H. V. Demir, *Small* **2019**, *15*, 1804854.
[11] H. Shen, Q. Gao, Y. Zhang, Y. Lin, Q. Lin, Z. Li, L. Chen, Z. Zeng, X. Li, Y. Jia, S. Wang, Z. Du, L. S. Li, Z. Zhang, *Nat. Photonics* **2019**, *13*, 192.
[12] Y.-S. Park, J. Roh, B. T. Diroll, R. D. Schaller, V. I. Klimov, *Nat. Rev. Mater.* **2021**, *6*, 382.
[13] J. Song, O. Wang, H. Shen, Q. Lin, Z. Li, L. Wang, X. Zhang, L. S. Li, *Adv. Funct. Mater.* **2019**, *29*, 1808377.
[14] W. Cao, C. Xiang, Y. Yang, Q. Chen, L. Chen, X. Yan, L. Qian, *Nat. Commun.* **2018**, *9*, 2608.
[15] E. Jang, H. Jang, *Chem. Rev.* **2023**, *123*, 4663.
[16] W. D. Kim, D. Kim, D.-E. Yoon, H. Lee, J. Lim, W. K. Bae, D. C. Lee, *Chem. Mater.* **2019**, *31*, 3066.
[17] J. Frischeisen, D. Yokoyama, A. Endo, C. Adachi, W. Brütting, *Org. Electron.* **2011**, *12*, 809.
[18] W. Brütting, J. Frischeisen, T. D. Schmidt, B. J. Scholz, C. Mayr, *Phys. Status Solidi A* **2013**, *210*, 44.
[19] P. Bai, A. Hu, Y. Liu, Y. Jin, Y. Gao, *J. Phys. Chem. Lett.* **2020**, *11*, 4524.
[20] O. Erdem, S. Foroutan, N. Gheshlaghi, B. Guzelturk, Y. Altintas, H. V. Demir, *Nano Lett.* **2020**, *20*, 6459.
[21] P. Bai, A. Hu, Y. Deng, Z. Tang, W. Yu, Y. Hao, S. Yang, Y. Zhu, L. Xiao, Y. Jin, Y. Gao, *J. Phys. Chem. Lett.* **2022**, *13*, 9051.
[22] S. Ithurria, M. D. Tessier, B. Mahler, R. P. Lobo, B. Dubertret, A. L. Efros, *Nat. Mater.* **2011**, *10*, 936.
[23] R. Scott, J. Heckmann, A. V. Prudnikau, A. Antanovich, A. Mikhailov, N. Owschimikow, M. Artemyev, J. I. Climente, U. Woggon, N. B. Grosse, A. W. Achtstein, *Nat. Nanotechnol.* **2017**, *12*, 1155.
[24] Y. Gao, M. C. Weidman, W. A. Tisdale, *Nano Lett.* **2017**, *17*, 3837.
[25] F. Feng, L. T. Nguyen, M. Nasilowski, B. Nadal, B. Dubertret, A. Maître, L. Coolen, *ACS Photonics* **2018**, *5*, 1994.
[26] B. Liu, Y. Altintas, L. Wang, S. Shendre, M. Sharma, H. Sun, E. Mutlugun, H. V. Demir, *Adv. Mater.* **2020**, *32*, 1905824.
[27] Y. Kelestemur, Y. Shynkarenko, M. Anni, S. Yakunin, M. L. De Giorgi, M. V. Kovalenko, *ACS Nano* **2019**, *13*, 13899.
[28] S. Hu, F. Shabani, B. Liu, L. Zhang, M. Guo, G. Lu, Z. Zhou, J. Wang, J. C. Huang, Y. Min, Q. Xue, H. V. Demir, C. Liu, *ACS Nano* **2022**, *16*, 10840.
[29] F. Shabani, H. Dehghanpour Baruj, I. Yurdakul, S. Delikanli, N. Gheshlaghi, F. Isik, B. Liu, Y. Altintas, B. Canımkurbey, H. V. Demir, *Small* **2022**, *18*, 2106115.
[30] U. Giovanella, M. Pasini, M. Lorenzon, F. Galeotti, C. Lucchi, F. Meinardi, S. Luzzati, B. Dubertret, S. Brovelli, *Nano Lett.* **2018**, *18*, 3441.
[31] D.-E. Yoon, S. Yeo, H. Lee, H. Cho, N. Wang, G.-M. Kim, W. K. Bae, Y. K. Lee, Y.-S. Park, D. C. Lee, *Chem. Mater.* **2022**, *34*, 9190.
[32] A. Hu, P. Bai, Y. Zhu, Z. Tang, L. Xiao, Y. Gao, *Small* **2022**, *18*, 2204120.
[33] Z. Chen, B. Nadal, B. Mahler, H. Aubin, B. Dubertret, *Adv. Funct. Mater.* **2014**, *24*, 295.
[34] H. D. Baruj, I. Bozkaya, B. Canimkurbey, A. T. Isik, F. Shabani, S. Delikanli, S. Shendre, O. Erdem, F. Isik, H. V. Demir, *Small* **2023**, *19*, 2206582.
[35] K.-H. Kim, J.-J. Kim, *Adv. Mater.* **2018**, *30*, 1705600.
[36] J. W. Sun, J.-H. Lee, C.-K. Moon, K.-H. Kim, H. Shin, J.-J. Kim, *Adv. Mater.* **2014**, *26*, 5684.

[37] T.-A. Lin, T. Chatterjee, W.-L. Tsai, W.-K. Lee, M.-J. Wu, M. Jiao, K.-C. Pan, C.-L. Yi, C.-L. Chung, K.-T. Wong, C.-C. Wu, *Adv. Mater.* **2016**, *28*, 6976.
[38] K. Tsai, M. Hung, Y. Mao, S. Chen, *Adv. Funct. Mater.* **2019**, *29*, 1901025.
[39] K.-H. Kim, E. S. Ahn, J.-S. Huh, Y.-H. Kim, J.-J. Kim, *Chem. Mater.* **2016**, *28*, 7505.
[40] K.-H. Kim, J.-Y. Ma, C.-K. Moon, J.-H. Lee, J. Y. Baek, Y.-H. Kim, J.-J. Kim, *Adv. Opt. Mater.* **2015**, *3*, 1191.
[41] Y. Altintas, K. Gungor, Y. Gao, M. Sak, U. Quliyeva, G. Bappi, E. Mutlugun, E. H. Sargent, H. V. Demir, *ACS Nano* **2019**, *13*, 10662.
[42] A. A. Rossinelli, H. Rojo, A. S. Mule, M. Aellen, A. Cocina, E. De Leo, R. Schäublin, D. J. Norris, *Chem. Mater.* **2019**, *31*, 9567.
[43] O. Erdem, K. Gungor, B. Guzelturk, I. Tanriover, M. Sak, M. Olutas, D. Dede, Y. Kelestemur, H. V. Demir, *Nano Lett.* **2019**, *19*, 4297.
[44] R. Momper, H. Zhang, S. Chen, H. Halim, E. Johannes, S. Yordanov, D. Braga, B. Blülle, D. Doblas, T. Kraus, M. Bonn, H. I. Wang, A. Riedinger, *Nano Lett.* **2020**, *20*, 4102.
[45] Z. Wen, P. Liu, J. Ma, S. Jia, X. Xiao, S. Ding, H. Tang, H. Yang, C. Zhang, X. Qu, B. Xu, K. Wang, K. L. Teo, X. W. Sun, *Adv. Electron. Mater.* **2021**, *7*, 2000965.
[46] B. Liu, S. Delikanli, Y. Gao, D. Dede, K. Gungor, H. V. Demir, *Nano Energy* **2018**, *47*, 115.
[47] M. A. Lieb, J. M. Zavislan, L. Novotny, *J. Opt. Soc. Am. B* **2004**, *21*, 1210.
[48] J. A. Schuller, S. Karaveli, T. Schiros, K. He, S. Yang, I. Kymissis, J. Shan, R. Zia, *Nat. Nanotechnol.* **2013**, *8*, 271.
[49] N. F. Hartmann, M. Otten, I. Fedin, D. Talapin, M. Cygorek, P. Hawrylak, M. Korkusinski, S. Gray, A. Hartschuh, X. Ma, *Nat. Commun.* **2019**, *10*, 3253.
[50] T. Lee, B. J. Kim, H. Lee, D. Hahm, W. K. Bae, J. Lim, J. Kwak, *Adv. Mater.* **2022**, *34*, 2106276.